Inorganic Chemistry
Article

Inorg. Chem. **2009**, *48*, 10193–10201 **10193**
DOI: 10.1021/ic901655m

Facile Chemical Conversion Synthesis and Luminescence Properties of Uniform Ln^{3+} (Ln = Eu, Tb)-Doped $NaLuF_4$ Nanowires and $LuBO_3$ Microdisks

Guang Jia, Hongpeng You,* Yanhua Song, Junjiao Jia, Yuhua Zheng, Lihui Zhang, Kai Liu, and Hongjie Zhang*

State Key Laboratory of Rare Earth Resource Utilization, Changchun Institute of Applied Chemistry, Chinese Academy of Sciences, Changchun 130022, P. R. China, and Graduate University of the Chinese Academy of Sciences, Beijing 100049, P. R. China

Received June 18, 2009

Uniform $NaLuF_4$ nanowires and $LuBO_3$ microdisks have been successfully prepared by a designed chemical conversion method. The lutetium precursor nanowires were first prepared through a simple hydrothermal process. Subsequently, uniform $NaLuF_4$ nanowires and $LuBO_3$ microdisks were synthesized at the expense of the precursor by a hydrothermal conversion process. The whole process was carried out in aqueous condition without any organic solvents, surfactant, or catalyst. The conversion processes from precursor to the final products have been investigated in detail. The as-obtained Eu^{3+} and Tb^{3+}-doped $LuBO_3$ microdisks and $NaLuF_4$ nanowires show strong characteristic red and green emissions under ultraviolet excitation or low-voltage electron beam excitation. Moreover, the luminescence colors of the Eu^{3+} and Tb^{3+} codoped $LuBO_3$ samples can be tuned from red, orange, yellow, and green-yellow to green by simply adjusting the relative doping concentrations of the activator ions under a single wavelength excitation, which might find potential applications in the fields such as light display systems and optoelectronic devices.

1. Introduction

Nano/microstructures with well-defined shapes have attracted increasing interest, and they are expected to be very useful in a wide range of applications, such as nanoelectronics, information storage, catalysis, and biosensors. The preparation of nano/microsized inorganic materials with specific morphology, which may have a great influence on their physical properties, is required to meet different scientific and technological needs.[1−3] A variety of materials with different shapes and sizes have been prepared such as nanowires,[4] nanorods,[5] nanotubes,[6] nanocubes,[7] nanopyramids,[8] nanotriangles,[9] and nanoplates.[10] Recently, a number of synthesis techniques have been developed to synthesize nano/submicrocrystals with uniform morphology, such as solvothermal technique, sol−gel route, polyol process, chemical vapor synthesis, coprecipitation method, and sonochemical synthesis. Besides all these methods, a promising chemical conversion route (sacrificial precursor method) has drawn our great attention.[11−14] To date, some well-defined nano/microcrystals, especially various hollow structures and one-dimensional nanomaterials, have been successfully prepared by this conversion route.[15−27] During the reaction, the

*E-mail: hpyou@ciac.jl.cn (H.Y.), hongjie@ciac.jl.cn (H.Z.).

(1) El-Sayed, M. A. *Acc. Chem. Res.* **2001**, *34*, 257.
(2) Alivisatos, A. P. *Science* **1996**, *271*, 933.
(3) Williams, F.; Nozik, A. J. *Nature* **1984**, *312*, 21.
(4) Morales, A. M.; Liber, C. M. *Science* **1998**, *279*, 208.
(5) Peng, X. G.; Manna, L.; Yang, W. D.; Wickham, J.; Scher, E.; Kadavanish, A.; Alivisatos, A. P. *Nature* **2000**, *404*, 59.
(6) Song, S. Y.; Zhang, Y.; Xing, Y.; Wang, C.; Feng, J.; Shi, W. D.; Zheng, G. L.; Zhang, H. J. *Adv. Funct. Mater.* **2008**, *18*, 2328.
(7) Ahmadi, T. S.; Wang, Z. L.; Green, T. C.; Henglein, A.; El-sayed, M. A. *Science* **1996**, *272*, 1924.
(8) Zhang, X.; Tsuji, M.; Lim, S.; Miyamae, N.; Nishio, M.; Hikino, S.; Umezu, M. *Langmuir* **2007**, *23*, 6372.
(9) Rai, A.; Singh, A.; Ahmad, A.; Sastry, M. *Langmuir* **2006**, *22*, 736.
(10) Shi, W. D.; Zhou, L.; Song, S. Y.; Yang, J. H.; Zhang, H. *J. Adv. Mater.* **2008**, *20*, 1892.
(11) Liang, H. P.; Zhang, H. M.; Hu, J. S.; Guo, Y. G.; Wan, L. J.; Bai, C. L. *Angew. Chem., Int. Ed.* **2004**, *43*, 1540.
(12) Sun, Y. G.; Xia, Y. N. *Adv. Mater.* **2004**, *16*, 264.
(13) Sun, Y. G.; Xia, Y. N. *J. Am. Chem. Soc.* **2004**, *126*, 3892.
(14) Metraux, G. S.; Cao, Y. C.; Jin, R. C.; Mirkin, C. A. *Nano Lett.* **2003**, *3*, 519.
(15) Yin, Y. D.; Rioux, R. M.; Erdonmez, C. K.; Hughes, S.; Somorjai, G. A.; Alivisatos, A. P. *Science* **2004**, *304*, 711.
(16) Peng, Q.; Xu, S.; Zhuang, Z. B.; Wang, X.; Li, Y. D. *Small* **2005**, *1*, 216.
(17) Wang, H. L.; Qi, L. M. *Adv. Funct. Mater.* **2008**, *18*, 1249.
(18) Yu, J. G.; Guo, H. T.; Davis, S. A.; Mann, S. *Adv. Funct. Mater.* **2006**, *16*, 2035.
(19) Dawood, F.; Schaak, R. E. *J. Am. Chem. Soc.* **2009**, *131*, 424.
(20) Gao, J. N.; Li, Q. H.; Zhao, H. B.; Li, L. S.; Liu, C. L.; Gong, Q. H.; Qi, L. M. *Chem. Mater.* **2008**, *20*, 6263.
(21) Chen, M. H.; Gao, L. *Inorg. Chem.* **2006**, *45*, 5145.
(22) Dloczik, L.; Konenkamp, R. *Nano Lett.* **2003**, *3*, 651.
(23) Gu, M.; Liu, Q.; Mao, S. P.; Mao, D. L.; Chang, C. K. *Cryst. Growth Des.* **2008**, *8*, 1422.
(24) Miao, J. J.; Jiang, L. P.; Liu, C.; Zhu, J. M.; Zhu, J. J. *Inorg. Chem.* **2007**, *46*, 5673.
(25) Jiao, S. H.; Jiang, K.; Zhang, Y. H.; Xiao, M.; Xu, L. F.; Xu, D. S. *J. Phys. Chem. C* **2008**, *112*, 3358.
(26) Ding, S.; Lu, P.; Zheng, J. G.; Yang, X. F.; Zhao, F. L.; Chen, J.; Wu, H.; Wu, M. M. *Adv. Funct. Mater.* **2007**, *17*, 1879.
(27) Jeong, U.; Camargo, P. H. C.; Leeb, Y. H.; Xia, Y. N. *J. Mater. Chem.* **2006**, *16*, 3893.

Published on Web 09/29/2009

precursors usually not only acted as the reactants but also controlled the shape of the products as a template.

Recently, much research attention has been paid to the synthesis of lanthanide compounds since they can be used for high efficient phosphors, catalysts, and other functional materials based on their novel electronic, optical, and chemical properties.[28−32] Controlled synthesis of well-defined lanthanide compounds with uniform dimensions and shape is of extraordinary importance because the electronic structure, bonding, surface energy, and chemical reactivity are directly related to their size and morphology. Up to now, numerous efforts have been devoted to the exploration of various convenient and efficient approaches for the fabrication of different kinds of lanthanide compounds. Among the various synthesis techniques, hydrothermal method as a typical solution approach has been proven to be a facile and general process for the synthesis of nano- and microsized lanthanide compounds with special morphologies and architectures.[31−34]

Recently, we have synthesized the uniform lutetium precursor $[Lu_4O(OH)_9(NO_3)]$ nanowires through a simple hydrothermal process without any organic solvents or surfactants.[35] In this paper, the as-obtained precursor has been successfully utilized to fabricate highly uniform $NaLuF_4$ nanowires and $LuBO_3$ microdisks by a facile hydrothermal conversion process. Furthermore, the formation process and luminescence properties of the as-synthesized lutetium compounds have been investigated in detail.

2. Experimental Section

$Ln(NO_3)_3$ (Ln = Lu and Eu) and $Tb(NO_3)_3$ aqueous solution were obtained by dissolving Ln_2O_3 (99.99%) and Tb_4O_7 (99.99%) in dilute HNO_3 solution under heating with agitation.

2.1. Synthesis of Precursor Nanowires. The lutetium precursors were prepared according to our previous work.[35] In a typical procedure, 4 mL of 0.5 M $Lu(NO_3)_3$ aqueous solution was added to 35 mL of deionized water. Then 25 wt % of ammonia solution was introduced to the solution until pH = 10. After additional agitation for 1 h, the as-obtained white colloidal suspension was transferred to a 50 mL autoclave and heated at 200 °C for 24 h. The precursor was washed for several times and redispersed in 10 mL of deionized water.

2.2. Synthesis of $NaLuF_4$ Nanowires. 0.5 g of NaF was dissolved in 35 mL of deionized water, and then 5 mL of the as-prepared precursor suspension was added with continuous stirring. After additional agitation for 30 min, the mixture was transferred to a 50 mL autoclave and maintained at 180 °C for 24 h. The white precipitate was obtained and washed with deionized water, centrifuged, and dried at 60 °C in air.

2.3. Synthesis of $LuBO_3$ Microdisks. 0.13 g of H_3BO_3 (2 mmol) was first dissolved in 35 mL of deionized water, and then 5 mL of the as-prepared precursor suspension was added with continuous stirring. After additional agitation for 30 min, the mixture was transferred to a 50 mL autoclave and maintained at 220 °C for 24 h. The white precipitate was washed with deionized water, centrifuged, and dried at 60 °C in air. A similar process was employed to prepare Eu^{3+} and Tb^{3+} doped lutetium compounds except for adding a stoichiometric amount of $Eu(NO_3)_3$, $Tb(NO_3)_3$ instead of $Lu(NO_3)_3$ aqueous solution at the initial stage.

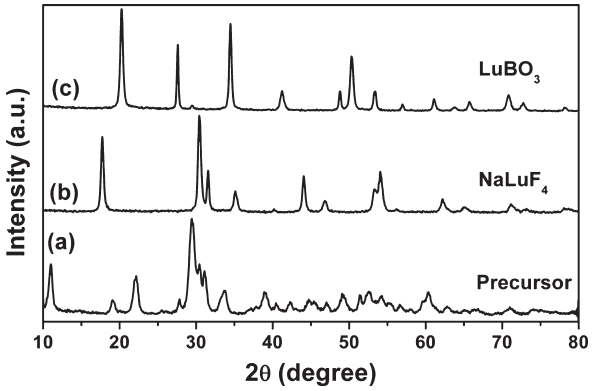

Figure 1. XRD patterns of (a) the precursor and the hydrothermal conversion products: (b) $NaLuF_4$ (180 °C, 24 h), and (c) $LuBO_3$ (220 °C, 24 h).

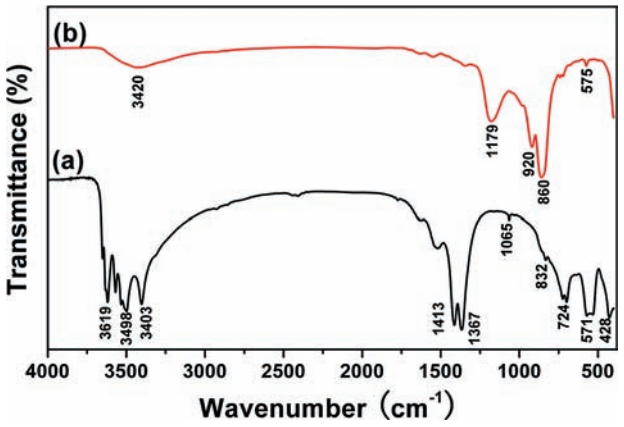

Figure 2. FT−IR spectra of (a) the precursor and (b) $LuBO_3$ microdisks.

For comparison, the bulk $LuBO_3$:Eu^{3+} and $LuBO_3$:Tb^{3+} samples were prepared by a normal solid-state reaction (SSR) using stoichiometric amounts of Lu_2O_3, Eu_2O_3, Tb_4O_7, and H_3BO_3 (50% excess) at 1300 °C for 2 h. The $LuBO_3$:Eu^{3+} sample was synthesized directly in air, and the $LuBO_3$:Tb^{3+} sample was obtained under a reducing atmosphere of CO.

2.4. Characterization. The samples were characterized by powder X-ray diffraction (XRD) performed on a D8 Focus diffractometer (Bruker). Fourier transform infrared spectroscopy (FT−IR) spectra were measured with a Perkin−Elmer 580B infrared spectrophotometer with the KBr pellet technique. The morphology of the samples was inspected using a scanning electron microscope (SEM; S-4800, Hitachi). Transmission electron microscopy (TEM) images and selected area electron diffraction (SAED) patterns were obtained using a JEOL 2010 transmission electron microscope operating at 200 kV. Photoluminescence (PL) excitation and emission spectra were recorded with a Hitachi F-4500 spectrophotometer equipped with a 150 W xenon lamp as the excitation source. The cathodoluminescence (CL) measurements were carried out in an ultrahigh-vacuum chamber ($< 10^{-8}$ Torr), and the spectra were recorded on an F-4500 spectrophotometer. The luminescence decay curves were obtained from a Lecroy Wave Runner 6100

(28) Xu, A. W.; Fang, Y. P.; You, L. P.; Liu, H. Q. *J. Am. Chem. Soc.* **2003**, *125*, 1494.
(29) Hu, C. G.; Liu, H.; Dong, W. T.; Zhang, Y. Y.; Bao, G.; Lao, C. S.; Wang, Z. L. *Adv. Mater.* **2007**, *19*, 470.
(30) Guan, M. Y.; Tao, F. F.; Sun, J. H.; Xu, Z. *Langmuir* **2008**, *24*, 8280.
(31) Wang, X.; Li, Y. D. *Angew. Chem., Int. Ed.* **2002**, *41*, 4790.
(32) Wang, X.; Li, Y. D. *Chem.—Eur. J.* **2003**, *9*, 5627.
(33) Wang, Z.; Qian, X. F.; Yin, J.; Zhu, Z. K. *Langmuir* **2004**, *20*, 3441.
(34) Lu, C. H.; Qi, L. M.; Yang, J. H.; Wang, X. Y.; Zhang, D. Y.; Xie, J. L.; Ma, J. M. *Adv. Mater.* **2005**, *17*, 2562.
(35) Jia, G.; Zheng, Y. H.; Liu, K.; Song, Y. H.; You, H. P.; Zhang, H. J. *J. Phys. Chem. C* **2009**, *113*, 153.

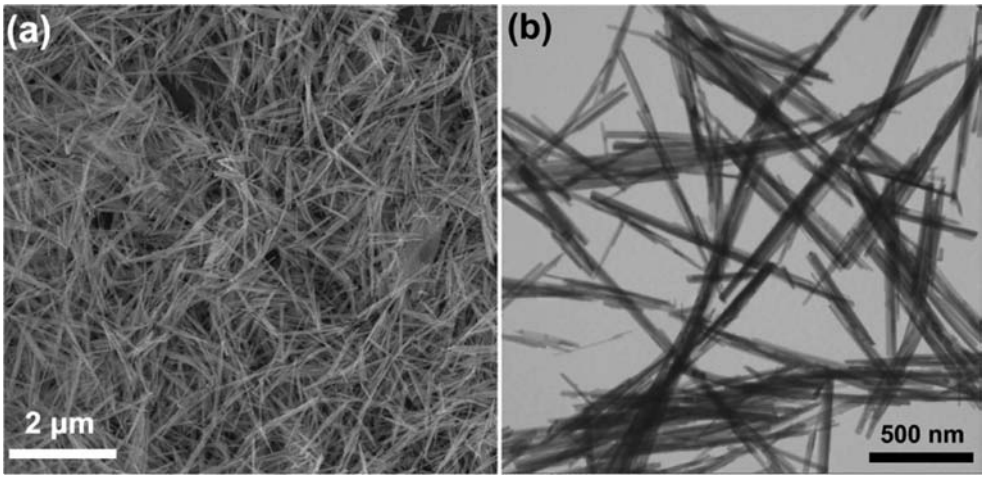

Figure 3. (a) SEM and (b) TEM images of the precursor.

Digital Oscilloscope (1 GHz) using a tunable laser (pulse width = 4 ns, gate = 50 ns) as the excitation (Continuum Sunlite OPO). All measurements were performed at room temperature.

3. Results and Discussion

3.1. Phase Identification and Morphology. Figure 1 shows the X-ray diffraction patterns of the precursor and the hydrothermal conversion products. It can be concluded from Figure 1a that the precursor has a structure of $Lu_4O(OH)_9(NO_3)$,[35] which is similar to the monoclinic phase of $Y_4O(OH)_9NO_3$ (JCPDS No. 79-1352).[36,37] After reacting with the NaF, or H_3BO_3 at designed hydrothermal conditions, the precursor can be converted to the pure phase of hexagonal $NaLuF_4$ (JCPDS No. 27-0726) and hexagonal $LuBO_3$ (JCPDS No. 74-1938), respectively (Figure 1b,c). No impurity peaks are observed, indicating the high purity of the final products. It can also be seen that the diffraction peaks of the $NaLuF_4$ and $LuBO_3$ samples are very sharp and strong, indicating that the products with high crystallinity can be synthesized by this method. This is important for phosphors, because high crystallinity generally means less traps and stronger luminescence.

Figure 2a shows the FT−IR spectrum of the as-obtained lutetium precursor. The absorption bands at about 724, 832, 1065, and 1367 cm^{-1} confirm the existence of the NO_3^- groups. The sharp bands in the range of 3450−3700 cm^{-1} are attributed to the stretching vibration of OH^- groups in the precursor. These results can support the structure $[Lu_4O(OH)_9(NO_3)]$ of the precursor.[35] Figure 2b shows the FT−IR spectra of the as-obtained $LuBO_3$ sample prepared at 220 °C for 24 h. It can be seen that the characteristic bands of the NO_3^- and OH^- groups of the precursor disappear after the hydrothermal conversion process. Instead, some intense bands in the range of 800−1200 cm^{-1} (centered at 860, 920, and 1179 cm^{-1}) appear (Figure 2b). The intense absorption bands can be attributed to the characteristic vibrational mode of the polyborate group $B_3O_9^{9-}$. The IR absorption bands at 860 and 920 cm^{-1} are assigned to ring-stretching vibration modes, and the peak at 1179 cm^{-1} is assigned to terminal stretching vibration modes.[38,39] A small peak near 575 cm^{-1} can be distinguished as an in-plane blending of the BO_4 group or the BO_3 group in vaterite-type borates.[39] The result provides additional evidence that the precursor has completely converted to the $LuBO_3$ sample after the hydrothermal process.

Figure 3 shows the SEM and TEM images observed from the as-formed hydrothermal precursor, clearly indicating that the lutetium precursor consists of uniform nanowires in 100% morphological yield. The result agrees well with the previous literature.[35] The uniform $NaLuF_4$ nanowires can be obtained by the conversion reaction of the wirelike lutetium precursor in the presence of NaF solution under the hydrothermal condition at 180 °C for 24 h. Figure 4a,b shows the SEM images of the $NaLuF_4$ sample, which indicate that the product consists of nanowires with diameters of 40−50 nm and lengths up to several micrometers in 100% morphological yield. The TEM images (Figure 4c,d) of the product are consistent with the SEM observations. In addition, it can be observed clearly from the TEM images that the uniform nanowires are very straight. As shown by the above results, one can see that both the precursor and $NaLuF_4$ nanowires have uniform size along each nanowire as well as a very smooth surface.

When the precursor reacted with H_3BO_3 under the hydrothermal condition at 220 °C for 24 h, the $LuBO_3$ product can be obtained (Figure 1). The SEM image with a low magnification (Figure 5a) reveals that the as-prepared $LuBO_3$ sample is entirely comprised of microdisks with a uniform size and well-defined round shape. As can be seen from the magnified SEM images (Figure 5b,c), the average diameter of the disks is about 2 μm. In addition, it can be clearly seen that the as-prepared $LuBO_3$ sample is composed of some thinner microdisks, and these thinner microdisks may be self-assembled into an integrated structure along the longitudinal axis direction through face-by-face attachment. TEM image (Figure 5d) further confirms the perfect round shape of the sample, which

(36) Christensen, A. N.; Nielsen, M.; O'Reilly, K. P. J.; Wroblewski, T. *Acta Chem. Scand.* **1992**, *46*, 224.
(37) Zhang, J.; Liu, Z. G.; Lin, J.; Fang, J. Y. *Cryst. Growth Des.* **2005**, *5*, 1527.
(38) Xu, Y. F.; Ma, D. K.; Chen, X. A.; Yang, D. P.; Huang, S. M. *Langmuir* **2009**, *25*, 7103.
(39) Yang, J.; Zhang, C. M.; Li, C. X.; Yu, Y. N.; Lin, J. *Inorg. Chem.* **2008**, *47*, 7262.

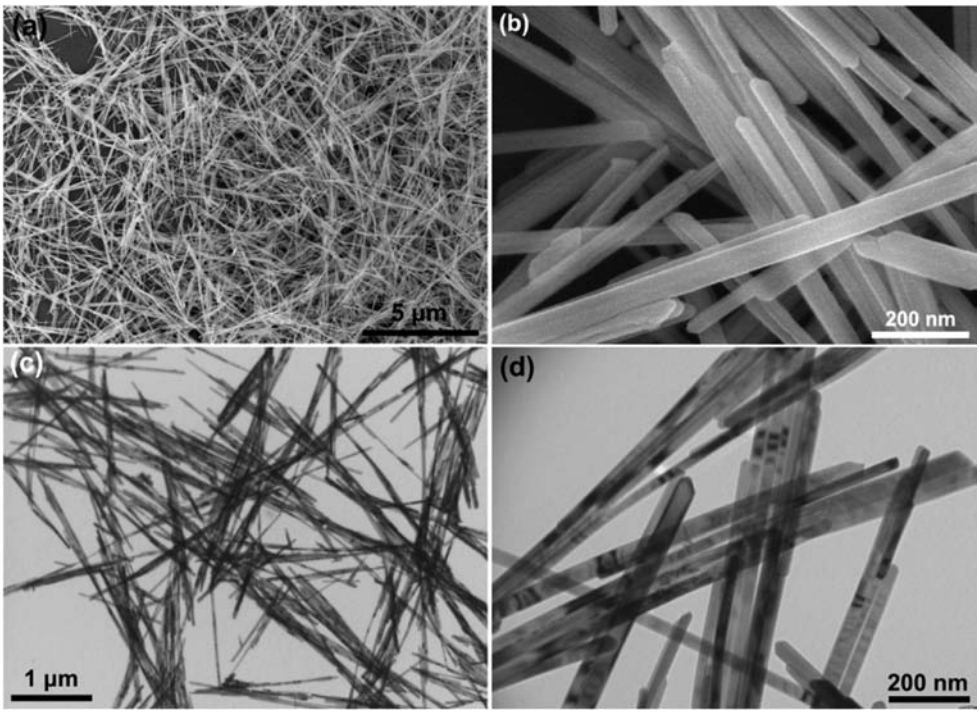

Figure 4. (a, b) SEM and (c, d) TEM images of the $NaLuF_4$ nanowires.

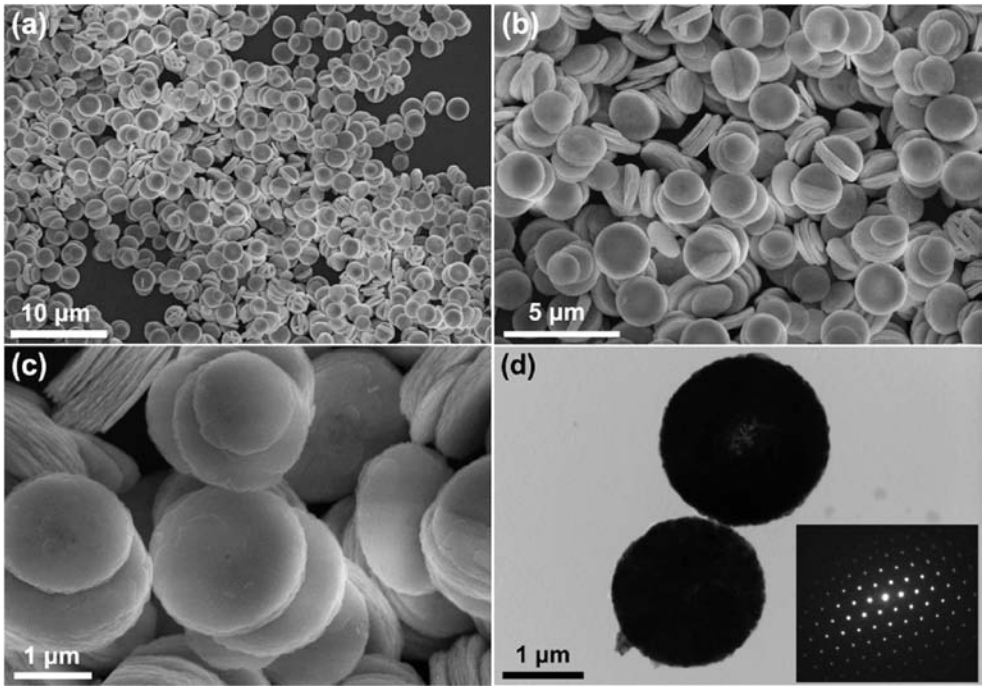

Figure 5. SEM images (a, b, c) and TEM image (d) of $LuBO_3$ microdisks. Inset in (d) is the corresponding SAED pattern taken from a single disk.

agrees well with the SEM observations. The SAED pattern (inset in Figure 5d) of a single disk shows the regular diffraction spots and confirms the single crystalline nature of the uniform microdisks.

3.2. Possible Formation Processes. On the basis of the results mentioned above, it can be seen that the uniform $NaLuF_4$ nanowires and $LuBO_3$ microdisks can be prepared by this simple hydrothermal conversion route from one single precursor. The possible formation mechanisms of the $NaLuF_4$ nanowires and $LuBO_3$ microdisks were investigated in detail. Generally, there are two possible ways to explain the formation process of the products prepared by the chemical conversion route. A possible explanation is the ordinary template-aided nucleation and subsequent crystal growth procedure. During the process, the reactant deposits on the surface of the precursor and gradually reacts with the inner core to form the products.[23,40,41]

(40) Aebischer, A.; Hostettler, M.; Hauser, J.; Kramer, K.; Weber, T.; Gudel, H. U.; Burgi, H. B. *Angew. Chem., Int. Ed.* **2006**, *45*, 2802.
(41) Zhang, F.; Zhao, D. Y. *ACS Nano* **2009**, *3*, 159.

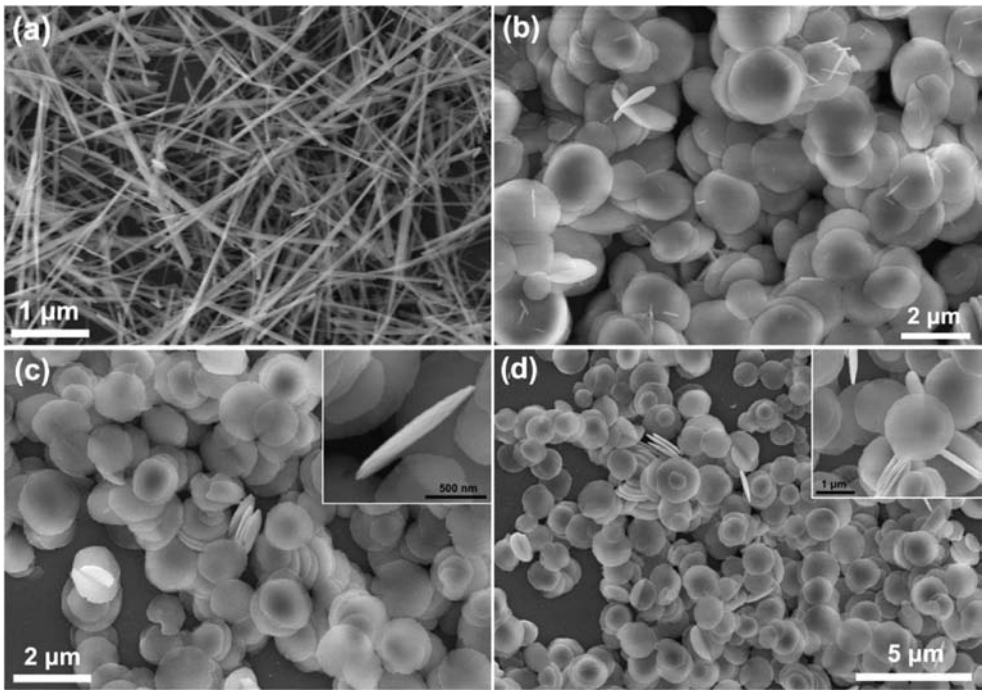

Figure 6. SEM images of the samples prepared at 220 °C for (a) 1 h, (b) 2 h, (c) 3 h, and (d) 6 h by using H_3BO_3 as reactant after the hydrothermal conversion process. Insets in (c) and (d) are the corresponding enlarged SEM images.

Another possible explanation is the dissolution-renucleation mechanism. In this process, the precursor dissolves gradually in solution and then reacts with the reactants to form new crystals of the products.[26,42,43]

In the present study, we hypothesize that the formation process of the $NaLuF_4$ nanowires can be expressed as an interface chemical transformation mechanism (the former mechanism). Up to now, some one-dimensional (1D) inorganic materials, such as $GdVO_4$ nanorods,[23] CdTe nanotubes,[24] and $CePO_4$ nanotubes,[44] have been successfully obtained by the interface chemical transformation process from their corresponding 1D precursors. During the conversion process, the precursors are employed as both the physical and chemical templates, which not only cast the morphology of the precursors but also afford a reactant source to initiate an interface reaction. In the formation process of the $NaLuF_4$ nanowires, the as-obtained products were formed by a surface deposition with a subsequent crystal growth procedure, during which the F^- and Na^+ ions in solution were deposited onto the surface of the lutetium precursor nanowires and then reacted gradually with the Lu^{3+} from the precursor to generate $NaLuF_4$. Furthermore, because in the hexagonal $NaLuF_4$ crystals Na^+ ions are randomly dispersed in different sites, they can be easily trapped into the crystals to form a more stable hexagonal phase of $NaLuF_4$ under the thermodynamic driving force effect.[41] Subsequently, the interface chemical transformation gradually continued to occur with the inner core in the hydrothermal conditions, resulting in the pure hexagonal $NaLuF_4$ nanowires.

The reaction time-dependent experiments were performed to investigate the conversion process of $LuBO_3$ microdisks. When the reaction was carried out at 220 °C for 1 h, the precursor was kept unchanged, and no $LuBO_3$ sample can be found (Figure 6a). By increasing the reaction time to 2 h, a large amount of $LuBO_3$ microdisks appeared immediately, and only a small quantity of the precursor existed, which adhered to the surfaces of $LuBO_3$ microcrystals (Figure 6b). It indicates that the formation process of the $LuBO_3$ sample is very fast. With the extension of the reaction time to 3 h or longer, the precursor disappeared completely and converted to pure $LuBO_3$ microdisks (Figure 6c,d). The result is in good accordance with the XRD results (Figure S1 in the Supporting Information). When the reaction was carried out for 6 h (Figure 6d), the diameters of the microdisks have no obvious change, but some single microdisks are stacked face to face (inset in Figure 6d). By increasing the reaction time to 24 h, the uniform and well-dispersed multilayered $LuBO_3$ microdisks are obtained (Figure 5). On the basis of the SEM results and analysis, it can be assumed that the original thinner microdisks are self-assembled into an integrated structure along the longitudinal axis direction through face-by-face attachment driven by the minimization of the total surface energy of the system (Figures 5 and 6). It indicates that the formation of the final thicker microdisks is the result of self-assembly of the round thinner microdisks via the oriented aggregation mechanism.[45−47] Moreover, the thinner microdisks that are assembled the multilayered microstructure are uniform in diameter. This phenomenon can also

(42) Xi, G. C.; Xiong, K.; Zhao, Q. B.; Zhang, R.; Zhang, H. B.; Qian, Y. T. *Cryst. Growth Des.* **2006**, *6*, 577.
(43) Yan, L.; Yu, R. B.; Chen, J.; Xing, X. R. *Cryst. Growth Des.* **2008**, *8*, 1474.
(44) Chen, G. Z.; Sun, S. X.; Zhao, W.; Xu, S. L.; You, T. *J. Phys. Chem. C* **2008**, *112*, 20217.
(45) Penn, R. L.; Banfield, J. F. *Science* **1998**, *281*, 969.
(46) Banfield, J. F.; Welch, S. A.; Zhang, H. Z.; Ebert, T. T.; Penn, R. L. *Science* **2000**, *289*, 751.
(47) Zitoun, D.; Pinna, N.; Frolet, N.; Belin, C. *J. Am. Chem. Soc.* **2005**, *127*, 15034.

Scheme 1. Schematic Illustration for the Possible Conversion Processes of $NaLuF_4$ Nanowires and $LuBO_3$ Microdisks

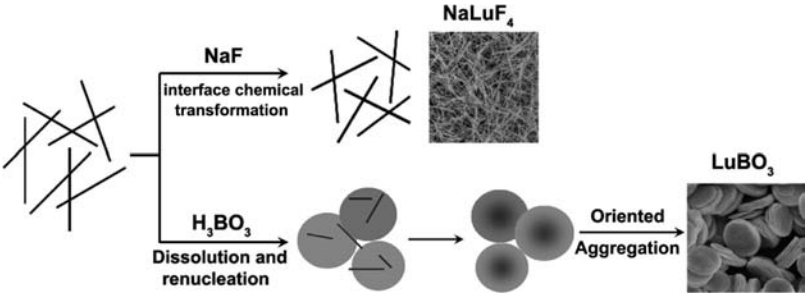

occur in the formation of LaF_3 and EuF_3 plate-built cylinders which are assembled by uniform LaF_3 and EuF_3 nanodisks.[48,49] On the basis of the reaction time-dependent evolution evidence, we can conclude that the conversion process from precursor nanowires to $LuBO_3$ microdisks can be rationally expressed as a dissolution-renucleation mechanism (the latter mechanism). A schematic illustration of the possible detailed conversion processes from the precursor nanowires to the final products is presented in Scheme 1.

3.3. Luminescence Properties. It is well-known that the lanthanide orthoborates and fluorides are very excellent host lattice for the luminescence of various optically active lanthanide ions.[38,39,41,50−52] However, for the study of luminescence, the lutetium compounds have been rarely studied.[53,54] Here, the luminescence properties of the Eu^{3+} and Tb^{3+} ions doped $LuBO_3$ microdisks and $NaLuF_4$ nanowires were investigated.

The XRD patterns of Eu^{3+} and Tb^{3+} doped $LuBO_3$ samples with different relative doping concentrations (Figure S2 in the Supporting Information) exhibit the peaks of pure hexagonal $LuBO_3$ (JCPDS No. 74-1938), indicating that the activator ions have been effectively doped into the $LuBO_3$ host lattice. Under short-wavelength UV light excitation, the as-obtained $LuBO_3$:Eu^{3+} and $LuBO_3$:Tb^{3+} samples exhibit strong red and green emissions, respectively. The photoluminescence (PL) excitation spectrum of the $LuBO_3$:5%Eu^{3+} sample consists of a strong absorption band centered at 235 nm and some weak lines, which are due to the charge transfer band between the O^{2-} and Eu^{3+} ions and the f−f transitions of the Eu^{3+} ions, respectively (Figure S3a in the Supporting Information). Upon excitation at 235 nm, the emission spectrum of $LuBO_3$:Eu^{3+} is composed of a group of lines at about 579, 591, 609 (627), 650 nm, which can be attributed to $^5D_0-^7F_J$ (J = 0, 1, 2, 3) transition lines of the Eu^{3+} ions, respectively (Figure 7a).[53] For comparison, the emission spectrum of bulk $LuBO_3$:5%Eu^{3+} sample prepared by solid-state reaction (SSR) is shown in Figure 7b. It can be clearly seen that the main peak positions in the emission spectra of the two samples are identical, but the relative intensity of $^5D_0-^7F_1$ and $^5D_0-^7F_2$ transitions of Eu^{3+} ions differ to some extent. The $LuBO_3$:5%Eu^{3+} sample prepared by the hydrothermal conversion method has a better chromaticity than that of the bulk sample, which can be confirmed by the CIE (Commission Internationale de I'Eclairage 1931) chromaticity diagram (points a and g in Figure 9). This improvement is especially important for a red phosphor-like $LuBO_3$:Eu^{3+}, whose application has always been restricted by its relatively poor chromaticity. The improvement of the color chromaticity can be attributed to the distinct microstructure of the assembly. The multilayered microdisks possess especially large surface areas and high surface energies, which would not only provide a driving force for the self-assembly but also result in a high degree of disorder near the surface and corresponding lower symmetry of crystal field around Eu^{3+} ions than in the bulk materials.[50,55] According to the Judd-Ofelt theory,[56] a lower symmetry of crystal field around Eu^{3+} ions would result in a higher R/O value (R = red, $^5D_0-^7F_2$; O = orange, $^5D_0-^7F_1$) and a higher color chromaticity.

The excitation spectrum of the $LuBO_3$:5%Tb^{3+} sample is mainly composed of two intense bands. The bands centered at 243 and 286 nm can be attributed to the spin-allowed transition (ΔS = 0) with higher energy and the spin-forbidden transition (ΔS = 1) with lower energy from the 4f to 5d of the Tb^{3+} ions, respectively (Figure S3b in the Supporting Information). Under excitation at 243 nm, the emission spectrum of $LuBO_3$:5%Tb^{3+} consists of a group of lines centered at about 488, 542, 582, and 618 nm, which corresponds to the $^5D_4-^7F_J$ (J = 6, 5, 4, 3) transitions of the Tb^{3+} ions, respectively (Figure 7c). From the emission spectrum of $LuBO_3$:5%Tb^{3+} prepared by the solid-state reaction (Figure 7d), we can see that the two emission spectra are basically identical. It is well-known that the Tb^{3+} ions can be easily oxidized during the calcination process in air, so the Tb^{3+} doped $LuBO_3$ sample should be synthesized in a reducing atmosphere at high temperature, which involves a complicated reaction process. In this case, the green-emitting $LuBO_3$:Tb^{3+} phosphor could be prepared by the hydrothermal conversion method without reducing atmosphere.

In order to investigate the tunable PL properties of the $LuBO_3$ microdisks, we have codoped Eu^{3+} and Tb^{3+} ions with different relative concentrations into $LuBO_3$ host lattice (total concentration: 5 mol %). The emission

(48) Cheng, Y.; Wang, Y. S.; Zheng, Y. H.; Qin, Y. *J. Phys. Chem. B* **2005**, *109*, 11548.
(49) Wang, M.; Huang, Q. L.; Hong, J. M.; Chen, X. T.; Xue, Z. L. *Cryst. Growth Des.* **2006**, *6*, 1972.
(50) Wang, L. Y.; Li, Y. D. *Nano Lett.* **2006**, *6*, 81645.
(51) Li, P.; Peng, Q.; Li, Y. D. *Adv. Mater.* **2009**, *21*, 1945.
(52) Wang, L. Y.; Li, Y. D. *Chem. Mater.* **2007**, *19*, 727.
(53) Yang, J.; Li, C. X.; Zhang, X. M.; Quan, Z. W.; Zhang, C. M.; Li, H. Y.; Lin, J. *Chem.—Eur. J.* **2008**, *14*, 4336.
(54) Li, C. X.; Yang, J.; Yang, P. P.; Zhang, X. M.; Lian, H. Z.; Lin, J. *Cryst. Growth Des.* **2008**, *8*, 923.
(55) Jiang, X. C.; Sun, L. D.; Feng, W.; Yan, C. H. *Cryst. Growth Des.* **2004**, *4*, 517.
(56) Judd, B. R. *Phys. Rev.* **1962**, *127*, 750.

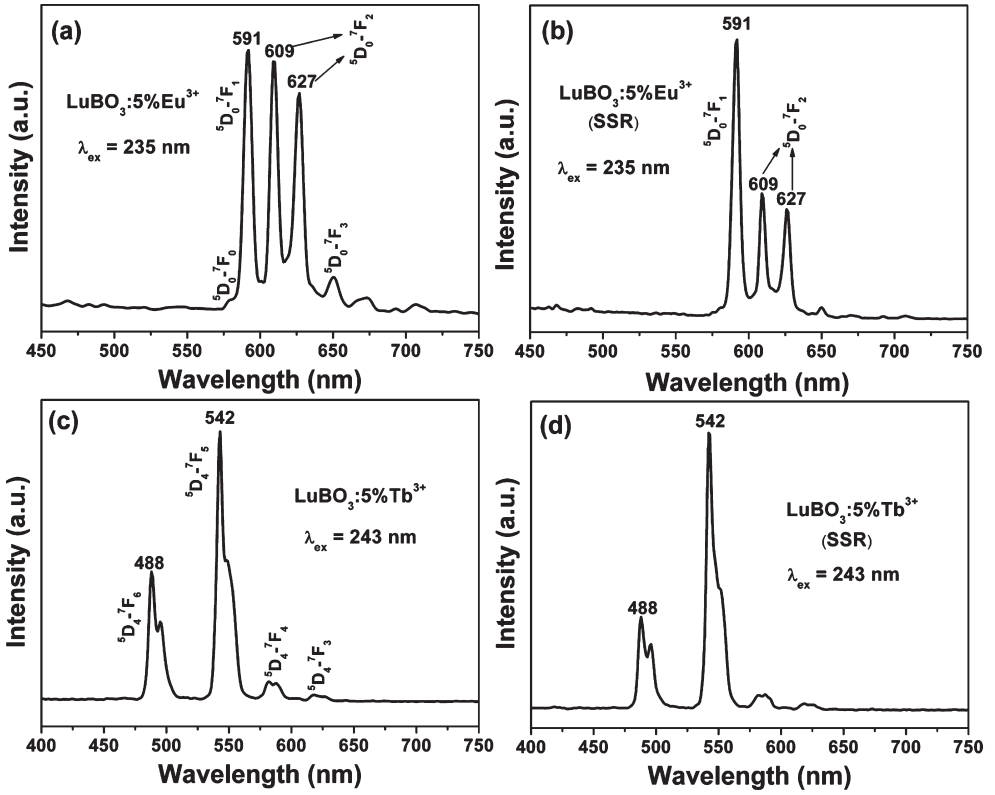

Figure 7. PL emission spectra of the as-prepared $LuBO_3$:5%Eu^{3+} (a, b) and $LuBO_3$:5%Tb^{3+} (c, d) samples prepared by the hydrothermal conversion method and solid-state reaction (SSR).

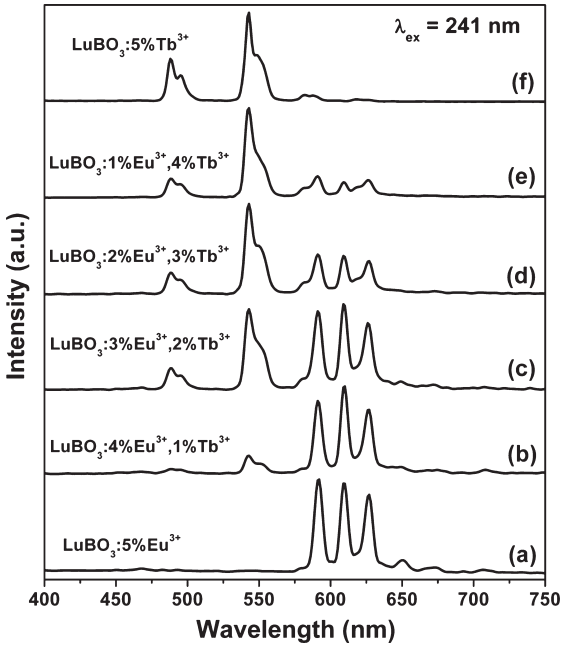

Figure 8. PL emission spectra of the Eu^{3+} and Tb^{3+} codoped $LuBO_3$ samples under the excitation at 241 nm (total concentration: 5 mol %).

spectra of the Eu^{3+} and Tb^{3+} codoped $LuBO_3$ samples under the excitation at 241 nm are shown in Figure 8. It can be seen that the as-obtained pure Eu^{3+} doped $LuBO_3$ sample shows strong red emission under UV light excitation. When the Tb^{3+} ions were doped into the $LuBO_3$ host lattice, the characteristic emission of the Tb^{3+} ions can be observed besides the Eu^{3+} emission. With increasing the relative concentration ratio of Tb^{3+}/Eu^{3+}, the luminescence of the Eu^{3+} ions gradually decreases, and that of Tb^{3+} increases obviously. Finally, the pure Tb^{3+} doped $LuBO_3$ sample shows bright green emission. As a result, the photoluminescence color can be tuned from red, orange, yellow, and green-yellow, to green by simply adjusting the relative doping concentrations of the Tb^{3+} and Eu^{3+} ions. The result can be confirmed by the corresponding CIE chromaticity diagram for the emission spectra of the $Eu^{3+}$and Tb^{3+} codoped $LuBO_3$ samples (Figure 9). This result indicates that the as-obtained phosphors could show merits of multicolor emissions in the visible region when excited by a single wavelength light, which might find potential applications in the fields such as light display systems and optoelectronic devices.

The photoluminescence properties of Eu^{3+} and Tb^{3+} doped $NaLuF_4$ nanowires were investigated (Figure S4 in the Supporting Information). The emission spectrum of the $NaLuF_4$:Eu^{3+} sample consists of the characteristic emission lines associated with the Eu^{3+} transitions from the excited $^5D_0$ levels to the ^7F_J (J = 1, 2, 3, 4) levels (Figure S4a in the Supporting Information). Upon excitation at 357 nm, the emission spectrum of the $NaLuF_4$:Tb^{3+} sample exhibits four obvious lines centered at 489, 546, 583, and 620 nm, originating from the transitions from the $^5D_4$ excited state to the ^7F_J (J = 6, 5, 4, 3) ground states of the Tb^{3+} ions, respectively (Figure S4b in the Supporting Information). The results agree well with the previous literature.[54]

The photoluminescence decay curves of the as-obtained phosphors were also investigated. The decay curves of the $LuBO_3$:Eu^{3+}, $LuBO_3$:Tb^{3+}, $NaLuF_4$:Eu^{3+}, and $NaLuF_4$:Tb^{3+} samples indicate that all the curves can

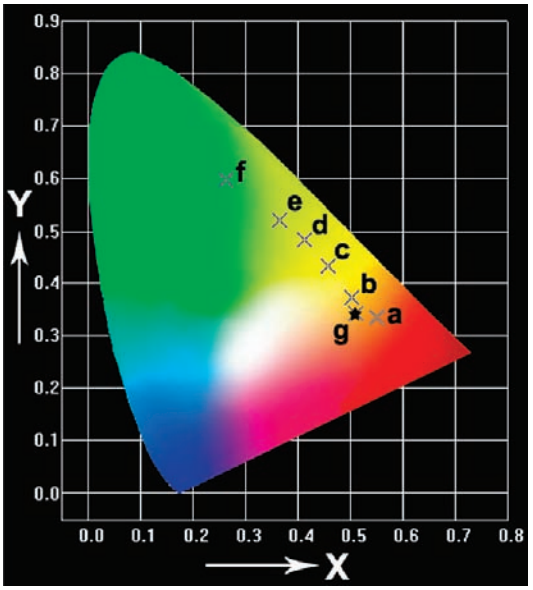

Figure 9. CIE chromaticity diagram for the emission spectra of the as-obtained Eu^{3+} and Tb^{3+} codoped $LuBO_3$ samples: (a) 5% Eu^{3+}; (b) 4% Eu^{3+}, 1% Tb^{3+}; (c) 3% Eu^{3+}, 2% Tb^{3+}; (d) 2% Eu^{3+}, 3% Tb^{3+}; (e) 1% Eu^{3+}, 4% Tb^{3+}; (f) 5% Tb^{3+}; and (g) the bulk $LuBO_3$:5% Eu^{3+} sample prepared by solid-state reaction (SSR).

be well fitted into a single exponential function as $I(t) = I_0 \exp(-t/\tau)$, in which τ is the decay lifetime. The lifetimes are determined to be 1.990, 5.037, 0.514, and 1.496 ms for $LuBO_3$:Eu^{3+}, $LuBO_3$:Tb^{3+}, $NaLuF_4$:Eu^{3+}, and $NaLuF_4$:Tb^{3+} samples, respectively (Figure S5 in the Supporting Information).

Figure 10 shows the typical cathodoluminescence (CL) spectra of $LuBO_3$:Eu^{3+} and $LuBO_3$:Tb^{3+} microdisks under the excitation of a low-voltage electron beam. It can be observed that the Eu^{3+}- and Tb^{3+}-doped $LuBO_3$ phosphors show strong red and green emissions under the excitation of low-voltage electron beam, and the CL spectra are basically identical with their corresponding PL emission spectra (Figure 7). However, the relative intensity of the emission peaks in photoluminescence and cathodoluminescence spectra varies, which may be caused by the different excitation mechanisms. The CL emission intensities for $LuBO_3$:5%Eu^{3+} and $LuBO_3$:5%Tb^{3+} phosphors were investigated as a function of the accelerating voltage and the filament current (Figure S6 in the Supporting Information). Under a 101 mA electron beam excitation, the CL intensities increase with rising the accelerating voltage from 2.5 to 4.5 kV (Figure S6a in the Supporting Information). Similarly, the CL intensities increase with increasing the filament current from 94 to 102 mA (Figure S6b in the Supporting Information) when the accelerating voltage is fixed at 3 kV. The increase in CL brightness with an increase in electron energy and filament current are attributed to a deeper penetration of electrons into the phosphor's body and the larger electron beam current density. For cathodoluminescence, the Eu^{3+} and Tb^{3+} ions are excited by the plasma produced by the incident electrons. With the increase of accelerating voltage or filament current, more plasma will be produced by the incident electrons, resulting in more excited activator ions and higher CL emission intensities. Due to the

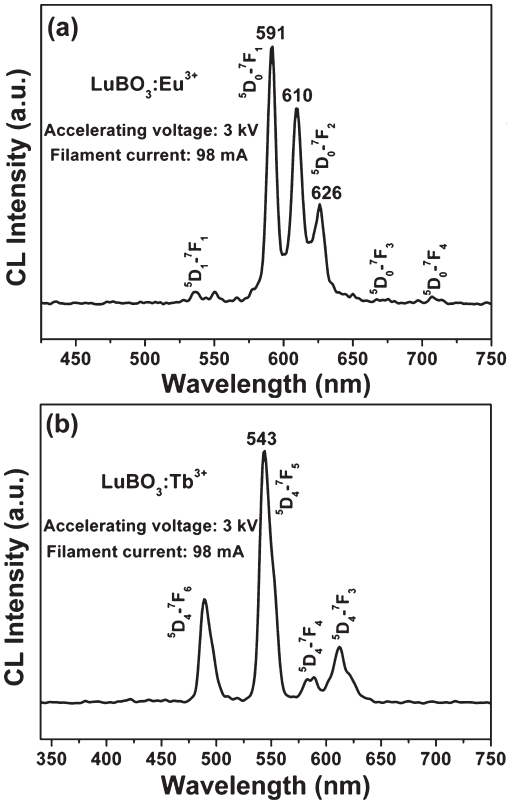

Figure 10. Typical CL spectra of (a) $LuBO_3$:5%Eu^{3+} and (b) $LuBO_3$:5%Tb^{3+} microdisks (accelerating voltage: 3 kV; filament current: 98 mA).

strong low voltage CL intensity and excellent dispersing properties of the phosphors, the Eu^{3+} and Tb^{3+} doped $LuBO_3$ microdisks are potentially applied in field emission display devices.

4. Conclusions

In summary, we highlight a general and facile chemical conversion method to fabricate uniform $NaLuF_4$ nanowires and $LuBO_3$ microdisks. The morphology, crystal structure, and luminescence properties were characterized by XRD, FT−IR, SEM, TEM, PL, CL, and kinetic decays, respectively. The possible mechanisms of the conversion process for the products have been discussed in detail. Under ultraviolet or low-voltage electron beam excitation, the Eu^{3+} and Tb^{3+} doped lutetium compounds show strong emissions with red and green colors, respectively. Moreover, the PL emission colors of the Eu^{3+} and Tb^{3+} codoped $LuBO_3$ microdisks can be tuned from red, orange, yellow, and green-yellow to green by adjusting the relative doping concentrations of the activator ions, which indicates that the as-obtained phosphors could show merits of multicolor emissions in the visible region when excited by a single wavelength excitation. Furthermore, this general and facile route may be of much significance in the synthesis of many other lanthanide compounds with various shapes.

Acknowledgment. This work is financially supported by the National Natural Science Foundation of China (Grant No. 20771098) and the National Basic Research Program of China (973 Program, Grant Nos. 2007CB935502 and 2006CB601103).

Supporting Information Available: XRD patterns of the as-obtained samples prepared at 220 °C for different reaction times by using H_3BO_3 as reactants (Figure S1); XRD patterns of Eu^{3+} and Tb^{3+} doped $LuBO_3$ samples with different relative doping concentrations (Figure S2); excitation spectra of the $LuBO_3$:5%Eu^{3+} and $LuBO_3$:5%Tb^{3+} microdisks (Figure S3); emission spectra of $NaLuF_4$:Eu^{3+} and $NaLuF_4$:Tb^{3+} nanowires (Figure S4); decay curves of the as-obtained phosphors (Figure S5); and CL emission intensities for $LuBO_3$:5%Eu^{3+} and $LuBO_3$:5%Tb^{3+} as a function of the accelerating voltage and the filament current (Figure S6). This material is available free of charge via the Internet at http://pubs.acs.org.